Journal of Alloys and Compounds 488 (2009) 448–453

Contents lists available at ScienceDirect

Journal of Alloys and Compounds

journal homepage: www.elsevier.com/locate/jallcom

Effect of MgO on structure and nonlinear dielectric properties of $Ba_{0.6}Sr_{0.4}TiO_3$/MgO composite ceramics prepared from superfine powders

Qing Xu[a,*], Xiao-Fei Zhang[a], Yu-Heng Huang[a], Wen Chen[a], Han-Xing Liu[a], Min Chen[b], Bok-Hee Kim[b]

[a] School of Materials Science and Engineering, Wuhan University of Technology, 122 Luoshi Road, Wuhan 430070, PR China
[b] Faculty of Advanced Materials Engineering, Chonbuk National University, Chonju 561756, Republic of Korea

ARTICLE INFO

Article history:
Received 6 July 2009
Received in revised form 25 August 2009
Accepted 26 August 2009
Available online 8 September 2009

Keywords:
Ceramics
Composite materials
Ferroelectrics
Oxide materials
Dielectric response

ABSTRACT

Composite ceramics with a nominal composition of $Ba_{0.6}Sr_{0.4}TiO_3$ + x wt.% MgO (x = 0–60) were prepared using superfine $Ba_{0.6}Sr_{0.4}TiO_3$ powder derived from a citrate method and superfine MgO powder. The sinterability, structure and nonlinear dielectric properties of the specimens were investigated. Adopting the superfine powders was found to be effective in promoting the sinterability of the composites. The specimens sintered at 1230 °C attained relative densities of around 95%. The relatively low sintering temperature of the composites suppressed the diffusion of Mg^{2+} into the lattice of the $Ba_{0.6}Sr_{0.4}TiO_3$ phase, which consequently led to a small shift of the temperature for dielectric constant maximum (T_m) to −10 °C. The variation of the nonlinear dielectric properties with MgO content was qualitatively interpreted in terms of doping and mixing effects caused by the MgO addition together with connectivity between the $Ba_{0.6}Sr_{0.4}TiO_3$ grains in the composites. At room temperature, the specimen with x = 60 showed a reduced dielectric constant of 420 and a low dielectric loss of 0.14% at 10 kHz, while maintained a roughly good tunability of 17.3% and a high figure of merit of 127 at 10 kHz and 20 kV/cm.

1. Introduction

In the past decades, barium strontium titanate ($Ba_{1-x}Sr_xTiO_3$, BST) has drawn increasing interest because of its strong dielectric nonlinearity under bias electric field and linearly adjustable Curie temperature with the strontium content over a wide temperature range. The desired properties make BST a promising candidate material for tunable microwave dielectric devices [1]. The applications of BST in the tunable microwave devices have been explored in various forms, such as bulk ceramics, thin films and thick films [1,2]. BST thick films exhibit the merits of lower fabrication costs compared with the thin films and smaller bias voltages required for tuning relative to the bulk ceramics. Fabricating BST thick films on alumina substrates by screen-printing or tape-casting has been believed to be cost-effective and flexible in view of mass production [3,4]. However, these thick films suffer from severe reactions with the substrates at high sintering temperatures [3,5]. Therefore, their sintering temperatures have to be limited to less than 1300 °C, which, in turn, leads to porous thick films with poor adhesion to the substrates [5]. Adding sintering aids, such as glass frits [5,6] and oxide additives [3,7], is an usually employed strategy to overcome the problem. Nevertheless, the reactions between BST thick films and the sintering aids may result in unfavorable changes in the structure and dielectric properties [6]. Thus, improving the sinterability of BST materials without adding the sintering aids emerges as an intriguing subject of practical importance. Adopting superfine starting powders with high reactivity is a viable approach to promote the sinterability of BST materials. There have been extensive researches on preparing superfine BST powders by various chemical solution methods, such as hydrothermal synthesis [8,9], sol–gel process [10], co-precipitation route [11] and citrate precursor method [12,13]. Our earlier work has revealed the effectiveness of adopting superfine $Ba_{0.6}Sr_{0.4}TiO_3$ powder derived from the citrate method in reducing the densification temperature and enhancing the overall nonlinear dielectric properties [13].

As well-known, a moderate dielectric constant, a low dielectric loss and a large tunability are preferred in light of the tunable microwave device applications. The relatively large dielectric constants and relatively high dielectric losses of BST are thus regarded to be undesired in view of the application requirements. Designing composite systems composed of BST and nonferroelectric components has been suggested to be efficient in diluting the dielectric constants and suppressing the dielectric losses [1]. Various nonferroelectric materials have been employed for this purpose, including MgO [1], Mg_2SiO_4 [14], Mg_2TiO_4 [15], Mg_2AlO_4 [16] and $MgTiO_3$ [17]. Magnesium can be viewed as a crucial constituent in these nonferroelectric materials from a chemical viewpoint. Thus, the role of magnesium on the structure and nonlinear dielectric properties appears as an investigation-worthy issue. Since the development of BST/MgO composites by Sengupta and Sengupta

* Corresponding author. Tel.: +86 27 87863277; fax: +86 27 87864580.
E-mail address: xuqing@whut.edu.cn (Q. Xu).

0925-8388/$ – see front matter © 2009 Elsevier B.V. All rights reserved.
doi:10.1016/j.jallcom.2009.08.153

[1], the composites have been the subject of extensive researches [18–22]. Moreover, the composite system has been used as the base for designing new BST-based composites by doping various oxides [23–25]. Despite these previous works, there have been few systematical researches on the relation between structural evolution and nonlinear dielectric property change for the composites with respect to the amount of added MgO. This thus warrants a further research on this subject from the viewpoint of elucidating contributing factors to the nonlinear dielectric properties, which may, in turn, offer a guideline to the design of novel BST-based composite systems. Furthermore, the majority of the previous works regarding the BST/MgO composites were conducted based on BST powders prepared by the solid-state reaction method and conventional MgO powder. It is thus necessary to investigate the feasibility and efficiency of improving the sinterability of the composites by using superfine BST and MgO powders with regard to their potential applications [5,21].

As has been well recognized, BST compositions with a paraelectric state at working temperatures are desirable from the viewpoint of tunable microwave device applications because of a good property combination including relatively high dielectric nonlinearity and relatively low dielectric loss [2]. Therefore, we prepared $Ba_{0.6}Sr_{0.4}TiO_3$/MgO composite ceramics using $Ba_{0.6}Sr_{0.4}TiO_3$ powder derived from the citrate method and superfine MgO powder. In this work, the sinterability, structure and nonlinear dielectric properties of the composite ceramics were examined in comparison with $Ba_{0.6}Sr_{0.4}TiO_3$ specimen.

2. Experimental

$Ba_{0.6}Sr_{0.4}TiO_3$ powder was synthesized by the citrate method using reagent grade $Ba(NiO_3)_2$ (Tianjin Kermel Chemical Reagent Co., Ltd.), $Sr(NiO_3)_2$ (Tianjin Fuchen Chemical Reagent Co., Ltd.), tetrabutyl titanate (Shanghai Experiment Reagent Co., Ltd.) and citric acid (Shanghai Experiment Reagent Co., Ltd.) as starting materials. Tetrabutyl titanate was first dissolved into a citric acid solution and various nitrates were then added, followed by stirring to yield a transparent aqueous solution. The mole ratio of citric acid to the total metal cation content was 1.25. The precursor solution was subjected to heating in an oven to form a foam-like solid precursor. The foam precursor was pulverized and calcined at 650 °C for 1 h in air. The detail of the synthesis process has been described elsewhere [13]. Superfine MgO powder (99.9%, Nanjing High Technology Nano Material Co., Ltd.) was mixed with the $Ba_{0.6}Sr_{0.4}TiO_3$ powder according to the nominal compositions of $Ba_{0.6}Sr_{0.4}TiO_3$ + x wt.% MgO (x = 0–60). After thorough mixing, the mixed powders were uniaxially pressed under a pressure of 300 MPa into discs of 19 mm in diameter and 1 mm in thickness. The compacted discs were subsequently sintered at 1230 °C for 2 h in air.

The phase purity of the BST powder and the crystal structure of the ceramic specimens were examined by a Philips X'pert PBO X-ray diffractometer using Cu K_α radiation. The morphology of the BST powder was observed at a Hitachi S-4700 field emission scanning electron microscope (FESEM). The specific surface area of the MgO powder was measured by the Brunauer–Emmett–Teller (BET) method using liquid nitrogen as the adsorbent. The dilatometric measurement of the compacted powders was conducted by a Netzsch DIL 402C dilatometer at a heating rate of 5 °C/min between 20 and 1400 °C in air. The microstructure of the ceramic specimens was observed using polished and thermally etched surfaces at a Jeol JSM-5610LV scanning electron microscope (SEM) attached with an energy dispersive spectroscopy (EDS) analyzer. The ceramic specimens were polished to ensure surface flatness. The bulk densities of the ceramic specimens were measured by the Archimedes method with ethyl alcohol as the medium. The theoretical densities of the composite specimens were estimated according to the mixing rule using the X-ray theoretical densities and volume fractions of the two constituents. The relative densities were determined from the measured and calculated data. The ceramic specimens were painted with silver paste on both surfaces as electrodes for measuring dielectric properties. The temperature dependence of the dielectric constant (ε_r) was measured by a HP4294 impedance analyzer and a JYT-800L environmental chamber between −60 and 120 °C. The nonlinear dielectric properties were measured at room temperature by a TH2818 automatic component analyzer at 10 kHz under external bias electric fields rising from 0 to 20 kV/cm.

3. Results and discussion

The X-ray diffraction (XRD) analysis identified a pure perovskite phase for the BST powder. The FESEM observation revealed that the BST powder was consisted of fine and uniform particles of around 100 nm. The characterization of the BST powder has been reported in our earlier paper [13]. The BET measurement showed a specific surface area of 11.2 m^2/g for the MgO powder. The average particle size of the MgO powder was determined to be 150 nm based on the BET datum. These results certified superfine morphology of the BST and MgO powders.

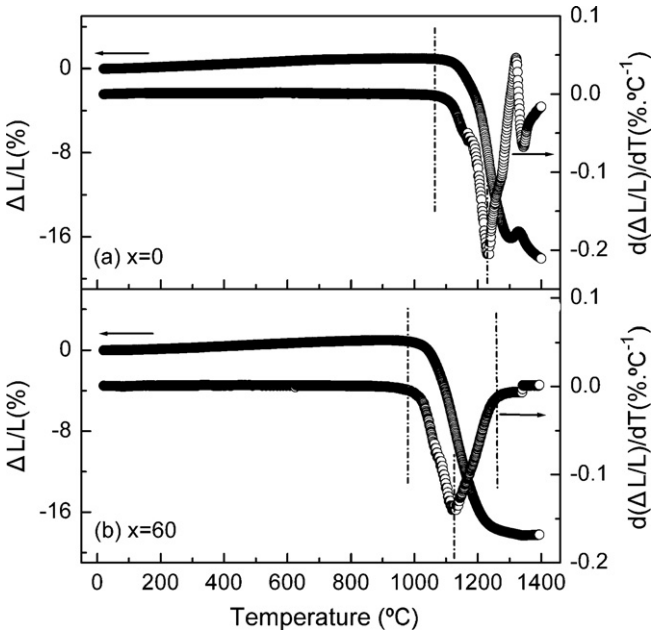

Fig. 1. Dilatometric curves of the compacted powders with (a) x = 0 and (b) x = 60.

Fig. 1 shows the dilatometric curves of the compacted powders with different MgO contents. The powder with x = 0 presented an onset temperature of shrinkage at around 1060 °C and a maximum shrinkage rate at 1220 °C (Fig. 1a). A small shoulder in the shrinkage ratio curve appeared at around 1320 °C, accompanied by an abrupt change of the shrinkage rate. It is considered to be caused by the generation of eutectic liquid phase [26]. By comparison, the shrinkage behavior of the composite powder with x = 60 occurred at lower temperatures, starting from about 980 °C, reaching a maximum rate at 1120 °C and tending to be saturated after 1260 °C (Fig. 1b). An obscure bumping in the shrinkage rate could be observed near 1320 °C, which is regarded to be due to the appearance of the eutectic liquid phase in the $Ba_{0.6}Sr_{0.4}TiO_3$ component of the composite specimen.

The dilatometric results hint that the powders could be sintered to reasonable densification levels at relatively low temperatures. As expected, the ceramic specimens with different MgO contents attained relative densities of around 95% after sintering at 1230 °C, as shown in Fig. 2. The relative densities of the specimens generally tended to rise with increasing MgO content. This tendency is in accordance with the dilatometric results in Fig. 1. A similar finding has been reported for $BaZr_{0.35}Ti_{0.65}O_3/MgTiO_3$ composite ceramics, with the $MgTiO_3$ addition serving to enhance the sinterability to a certain extent [27]. The specimen with x = 0 exhibited a relative density of 94.6%, which is roughly comparable with those of $Ba_{0.6}Sr_{0.4}TiO_3$ ceramics prepared by the conventional method and sintered at 1400 °C or higher temperatures [4,26]. The densification degree of the specimen is also quite close to those of $Ba_{0.6}Sr_{0.4}TiO_3$ ceramics added with 0.5 wt.% B_2O_3 as sintering aid and prepared using the conventional method by sintering at 1200–1300 °C [4]. Likewise, the sintering temperature of the composite specimens is obviously lower compared with literature data for BST/MgO composite ceramics. It has been reported that BST/MgO com-

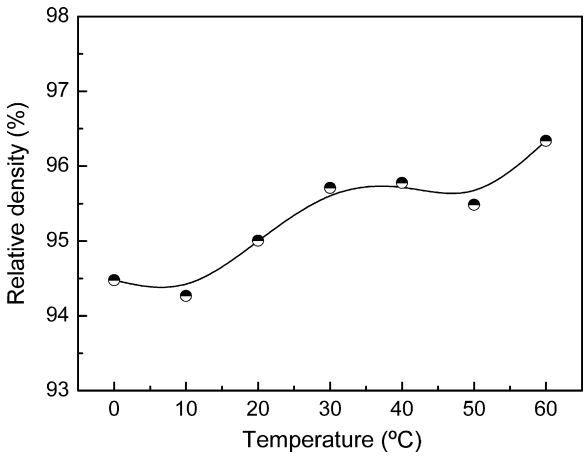

Fig. 2. Relative density of the ceramic specimens as a function of MgO content.

posite ceramics prepared from the conventional powders usually necessitate sintering temperatures of 1350–1550 °C for achieving reasonable densification [14,20,25]. Therefore, one can conclude that the $Ba_{0.6}Sr_{0.4}TiO_3$ and $Ba_{0.6}Sr_{0.4}TiO_3$/MgO powders have a high sintering reactivity. The improved sinterability of the specimens is assumed to be attributed to the superfine morphology of the BST and MgO powders.

Fig. 3 shows the SEM micrographs of the ceramic specimens with different MgO contents. In general, the specimens had dense microstructures. The specimen with $x = 0$ showed small and homogeneous grains of about 1 μm. Two sorts of grains distinct in contrast could be observed for the composite ceramics, with the light and dark grains being ascertained by the EDS analysis to be the $Ba_{0.6}Sr_{0.4}TiO_3$ and MgO phases, respectively. This assignation is consistent with previous results for BST/MgO composite ceramics [18–22]. Compared with the specimen with $x = 0$, the $Ba_{0.6}Sr_{0.4}TiO_3$ grains in the composite specimens became smaller, with the agglomerations of quite fine $Ba_{0.6}Sr_{0.4}TiO_3$ grains being observable. This result confirms the role of the MgO as a grain growth inhibitor for the $Ba_{0.6}Sr_{0.4}TiO_3$ in the composites [18]. Moreover, a generally good connectivity between the $Ba_{0.6}Sr_{0.4}TiO_3$ grains could be noticed for the composite specimens.

Fig. 4a shows the XRD patterns of the ceramic specimens with different MgO contents in the 2θ range of 20–80°. A pure perovskite structure with a cubic symmetry was identified for the ceramic specimen with $x = 0$. The composite specimens showed a diphase structure, composed of a cubic perovskite-structured $Ba_{0.6}Sr_{0.4}TiO_3$ phase and a cubic halite-structured MgO phase. This result indicates that chemical reaction between the two constituent phases during the sintering process appears to be insignificant. Carefully examining the XRD patterns in Fig. 4a, a shift of the XRD peaks corresponding to the $Ba_{0.6}Sr_{0.4}TiO_3$ phase in the composite specimens relative to the pure $Ba_{0.6}Sr_{0.4}TiO_3$ specimen ($x = 0$) could be distinguished. As a typical example, Fig. 4b evidenced the peak shift. The specimen of $x = 0$ presented a basically symmetrical peak within the 2θ range of 44–48°, assignable to the reflection from the (2 0 0) crystal plane of the cubic $Ba_{0.6}Sr_{0.4}TiO_3$. The composite specimens showed similar peaks, which can be attributed to the (2 0 0) plane reflection of the $Ba_{0.6}Sr_{0.4}TiO_3$ phase in the composites. Each composite specimen unambiguously displayed a peak shift towards a higher diffraction angle direction compared with the specimen with $x = 0$. Moreover, all the composite specimens maintained a

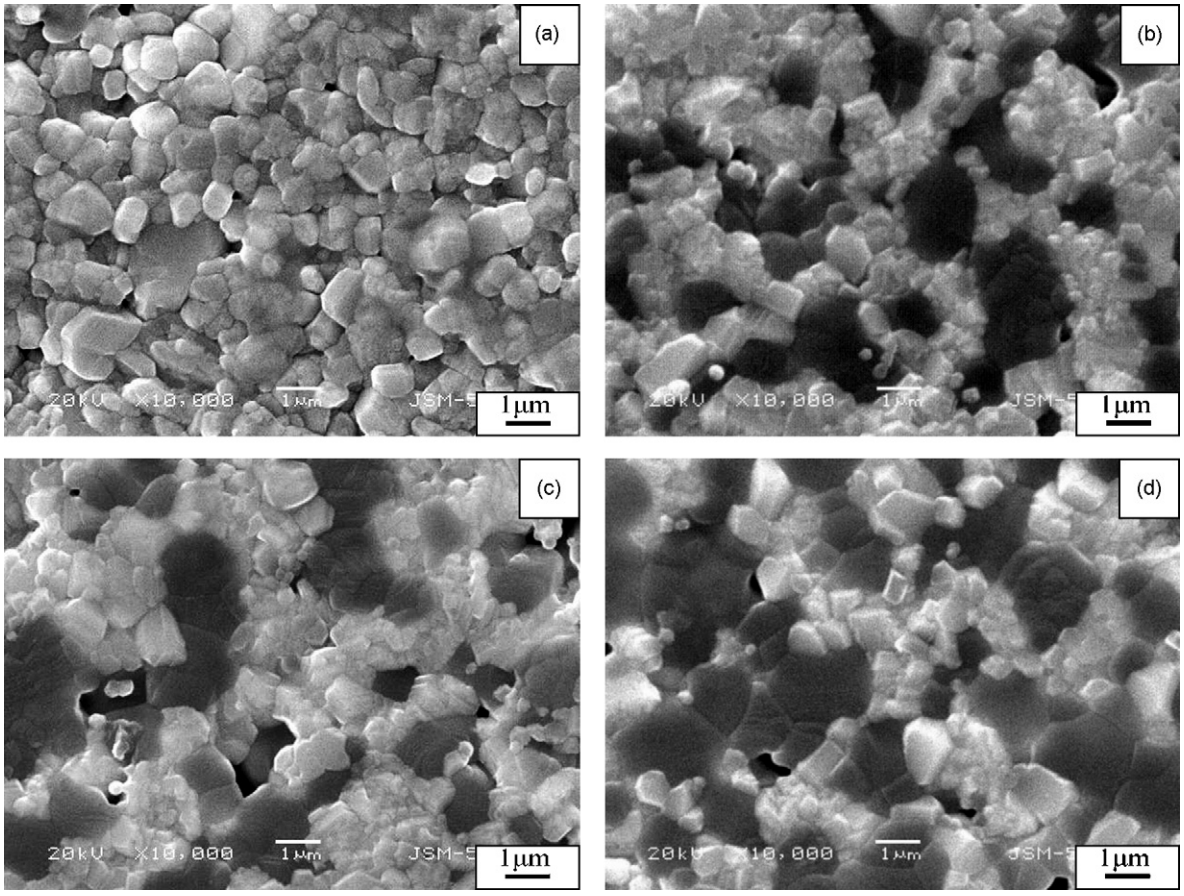

Fig. 3. SEM micrographs of the ceramic specimens with (a) $x = 0$, (b) $x = 30$, (c) $x = 50$ and (d) $x = 60$.

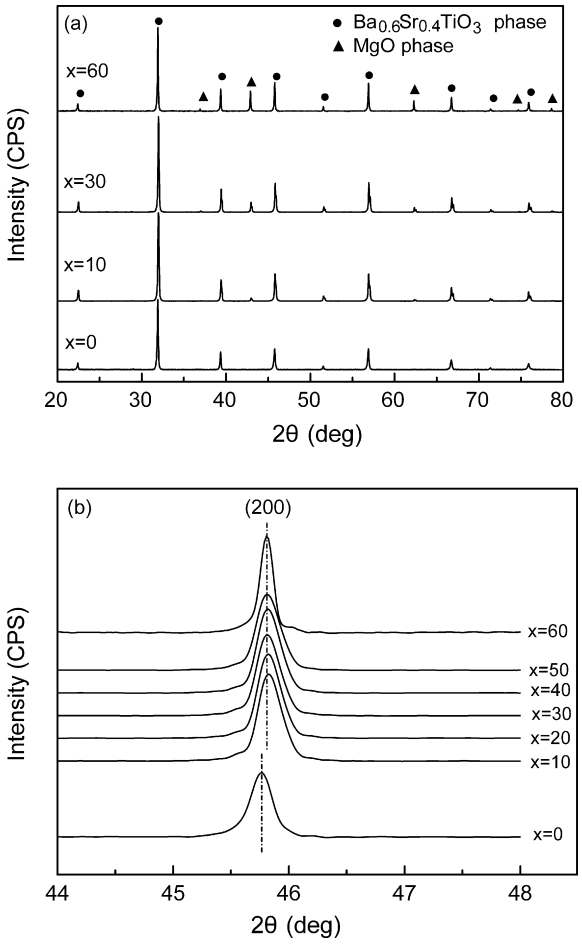

Fig. 4. XRD patterns of the ceramic specimens with different MgO contents in the 2θ ranges of (a) 20–80° and (b) 44–48°.

basically identical peak position regardless of the contents of added MgO.

The peak shift phenomenon can be qualitatively interpreted with respect to the incorporation of Mg^{2+} into the crystal structure of the $Ba_{0.6}Sr_{0.4}TiO_3$ phase. According to the Shannon's effective ionic radii, six-coordinate Mg^{2+} has a radius of 0.72 Å, which is close to that of six-coordinate Ti^{4+} (0.61 Å) [28]. Therefore, Mg^{2+} can diffuse into the six-fold coordinated site of the perovskite structure to substitute for Ti^{4+} because of radius matching. This doping behavior can be described by the following defect reaction equation using the Kröger–Vink notation:

$$MgO \xrightarrow{TiO_2} Mg''_{Ti} + V_O^{\bullet\bullet} + O_O \quad (1)$$

The substitution of relatively larger Mg^{2+} for relatively smaller Ti^{4+} can lead to an enlargement of the unit cells of the perovskite phase. On the other hand, the formation of oxygen vacancies to compensate for the heterovalent substitution can result in a contraction of the unit cells. The peak shift of the $Ba_{0.6}Sr_{0.4}TiO_3$ phase in the composite specimens relative to the specimen with $x=0$ appears to rely on the two-fold effect of the Mg^{2+} doping on the crystal structure. The present result indicates that the oxygen vacancy effect is likely to be predominant. The basically identical peak position of the composite specimens in Fig. 4b can be attributed to a low solubility of Mg^{2+} in the $Ba_{0.6}Sr_{0.4}TiO_3$ phase. It has been reported for $Ba_{0.6}Sr_{0.4}TiO_3$/MgO composite ceramics prepared by the conventional method that the solubility of MgO in the $Ba_{0.6}Sr_{0.4}TiO_3$ phase is well below a mixing content of 1.0 wt.% [18]. This value is far below the least addition amount of MgO in the present work.

Fig. 5 shows the temperature dependence of the dielectric constant (ε_r) at 10 kHz for the ceramic specimens with different MgO contents. The specimen with $x=0$ displayed a slightly diffused dielectric constant peak at around 0 °C, which is well consistent with a previously reported result for $Ba_{0.6}Sr_{0.4}TiO_3$ ceramic prepared by the conventional method [29]. As well-known, the dielectric constant anomaly is ascribed to a ferroelectric–paraelectric phase transition. The composite specimens showed a similar dielectric constant behavior. The dielectric constant peaks progressively became depressed and broadened with increasing MgO content. This behavior is attributed to the composite mixing effect of the nonferroelectric MgO phase, which diluted the ferroelectricity of the $Ba_{0.6}Sr_{0.4}TiO_3$ phase [20]. Compared with the specimen with $x=0$, the composite specimens presented a shift in the temperature of dielectric constant maximum (T_m) to a lower temperature of −10 °C. This result implies that the ferroelectric–paraelectric phase transition of the $Ba_{0.6}Sr_{0.4}TiO_3$ phase in the composites occurred at lower temperatures compared with the pure $Ba_{0.6}Sr_{0.4}TiO_3$ specimen ($x=0$). The T_m shift behavior can be explained in terms of the incorporation of Mg^{2+} into the lattice of the $Ba_{0.6}Sr_{0.4}TiO_3$ phase. As has been well recognized, the temperature stability of ferroelectricity of $Ba_{0.6}Sr_{0.4}TiO_3$ is closely associated with the magnitude of long-range coherent interactions between the ferroelectrically active [TiO_6] octahedra. The generation of oxygen vacancies due to the Mg^{2+} doping (Eq. (1)) can result in a detrimental effect on the long-range coupling between the oxygen octahedra. This effect is presumed to be responsible for the T_m lowering of the composite specimens. The composite specimens kept an invariant T_m whatever the MgO contents. This phenomenon can be attributed to the fact that the least content of MgO addition in the present work far exceeds the solubility of Mg^{2+} in the $Ba_{0.6}Sr_{0.4}TiO_3$ phase, which is consistent with the analysis result of Fig. 4b.

As suggested above, the T_m shift phenomenon was caused by the dissolution of a small amount of Mg^{2+} into the lattice of the $Ba_{0.6}Sr_{0.4}TiO_3$ phase. Thus, the degree of the T_m shift should be essentially related to the amount of Mg^{2+} dissolving into the lattice. Previous literature has reported various values of the T_m shift for $Ba_{0.6}Sr_{0.4}TiO_3$/MgO composite ceramics sintered under different conditions. Compared with the present work, $Ba_{0.6}Sr_{0.4}TiO_3$/MgO composite ceramics prepared by the conventional method and sintered at higher temperatures (e.g. 1550 °C) provided a larger shift of the T_m to a lower temperature of −30 °C [18,25]. A $Ba_{0.6}Sr_{0.4}TiO_3$/MgO composite ceramic prepared

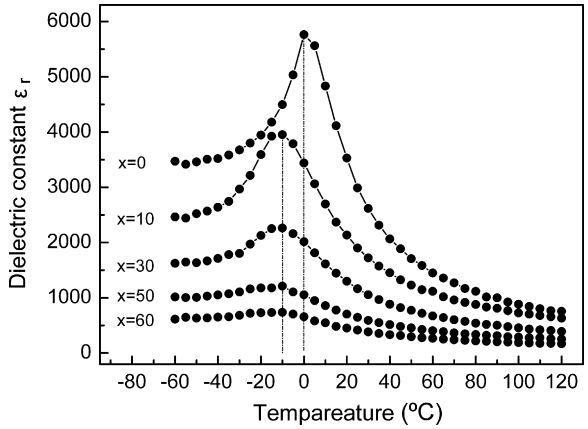

Fig. 5. Temperature dependence of the dielectric constant (ε_r) measured at 10 kHz for the ceramic specimens with different MgO contents.

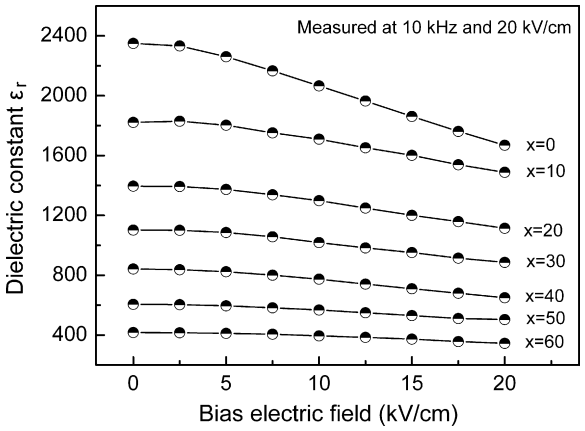

Fig. 6. Dielectric constant as a function of bias electric field for the ceramic specimens with different MgO contents.

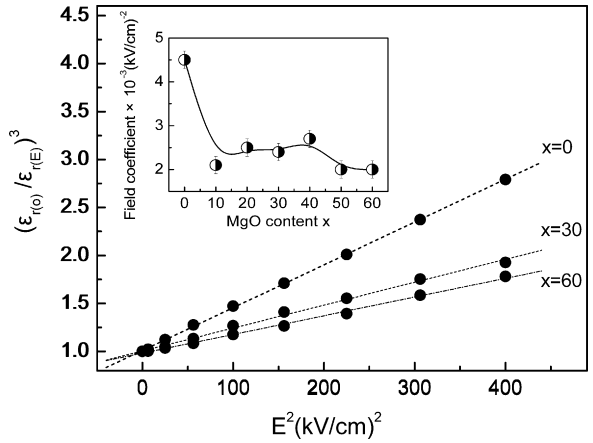

Fig. 7. $(\varepsilon_{r(0)}/\varepsilon_{r(E)})^3$ vs. E^2 plots of the ceramics specimens with different MgO contents. The inset shows the field coefficient of the specimens as a function of MgO content.

by microwave sintering at 1550 °C for 20 min offered a shift of the T_m to −52 °C [19]. In contrast, no shift of the T_m was detected for a $Ba_{0.6}Sr_{0.4}TiO_3$/MgO composite ceramic prepared by spark plasma sintering at 1200 °C for 3 min [22]. These comparisons suggest that the sintering conditions can greatly affect the kinetics of the Mg^{2+} diffusion and, as a result, determine the amount of Mg^{2+} dissolving into the lattice of the $Ba_{0.6}Sr_{0.4}TiO_3$ phase. Hence, one can argue that the relatively smaller shift of the T_m in the present work compared with the composite specimens prepared by the conventional method is attributable to a comparatively lower sintering temperature. In other words, the relatively low sintering temperature of the present work (1230 °C) depressed the diffusion of Mg^{2+} into the lattice of the $Ba_{0.6}Sr_{0.4}TiO_3$ phase.

Fig. 6 shows the dielectric constant as a function of bias electric field for the ceramic specimens with different MgO contents. In general, the dielectric constant of the specimen with $x = 0$ turned out to be smaller with increasing bias electric field, reflecting a typical feature of nonlinear dielectrics. The dielectric constants of the composite specimens showed an analogous bias electric field dependence. For the pure $Ba_{0.6}Sr_{0.4}TiO_3$ specimen ($x = 0$) with a paraelectric background at room temperature, a phenomenological equation has been confirmed to be valid to explicitly depict its dielectric constant nonlinearity [30,31]:

$$\frac{\varepsilon_{r(E)}}{\varepsilon_{r(0)}} = \frac{1}{[1 + \alpha\varepsilon_{r(0)}^3 E^2]^{1/3}} \quad (2)$$

where the $\varepsilon_{r(E)}$ and $\varepsilon_{r(0)}$ represent the dielectric constants under a bias electric field E and zero bias electric field, respectively, and the α is the phenomenological coefficient. The prefactor term of E^2, $\alpha\varepsilon_{r(0)}^3$, is defined as the field coefficient, quantifying the strength of the bias electric field effect [32]. Fig. 7 shows the $(\varepsilon_{r(0)}/\varepsilon_{r(E)})^3$ vs. E^2 plots of the ceramics specimens with different MgO contents. The specimen with $x = 0$ offered a linear plot, which is consistent well with the behavior predicted by Eq. (2). The dielectric constants of the composite specimens under bias electric fields also agree with the phenomenological expression. Note that the phenomenological expression was worked out to describe the electric field dependence of dielectric constant for polar dielectrics in a paraelectric state [30]. Thus, the good agreement of the dielectric constant data of the composite specimens with the phenomenological framework is believed to be attributed to the generally satisfactory connectivity between the $Ba_{0.6}Sr_{0.4}TiO_3$ grains in the composites (Fig. 3). The field coefficients of the specimens were determined from plot fitting, as shown in the inset of Fig. 7. The field coefficients displayed a rapid reduction from $x = 0$ to $x = 10$, followed by a slight decrement at the higher MgO contents.

Fig. 8 shows the nonlinear dielectric properties of the ceramic specimens with different MgO contents. The tunability was calculated as the percentage of dielectric constant change under the bias electric field of 20 kV/cm. The figure of merit (FOM), defined as tunability/tan δ, was determined from the data of the tunability and dielectric loss. The dielectric constants of the specimens monotonically decreased with increasing MgO content from 2350 ($x = 0$) to 420 ($x = 60$), which infers a dominant role of the mixing effect on the parameter. The dielectric losses (tan δ) showed a fluctuation around 0.25% at relatively low MgO contents ($x \leq 20$) and a steady decrement with increasing MgO content at the higher MgO contents ($x \geq 30$), with the specimens with $x = 60$ reaching a fairly low dielectric loss of 0.14%. This variation can be explained in view of the doping and mixing effects of added MgO. As aforementioned, the incorporation of a small amount of Mg^{2+} into the lattice of the $Ba_{0.6}Sr_{0.4}TiO_3$ phase of the composite specimens led to a shift of the T_m to −10 °C, which can correspondingly decrease the dielectric loss at room temperature. Meanwhile, the addition of nonferroelectric MgO with a low dielectric loss is favorable to depressing the dielectric loss of the composite specimens. One the other hand, the Mg^{2+} doping resulted in the creation of oxygen vacancies for charge balance purposes. The perovskite structure of $Ba_{0.6}Sr_{0.4}TiO_3$

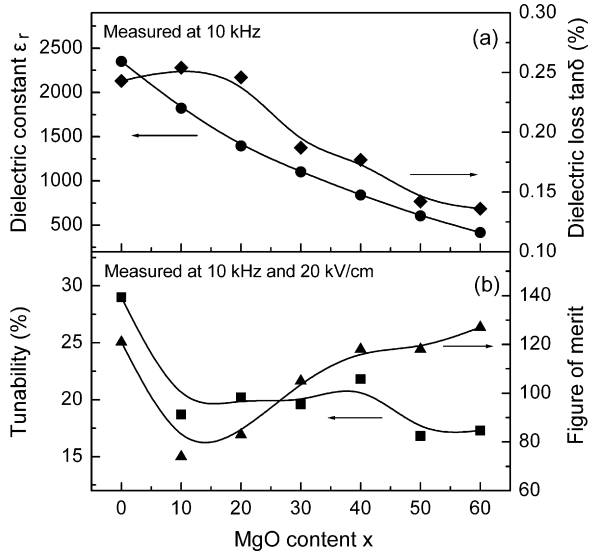

Fig. 8. Nonlinear dielectric properties of the ceramic specimens as a function of MgO content.

can be viewed as a network of [TiO_6] oxygen octahedra. The oxygen vacancies located at the corners of the octahedra can form complex-defect pairs or electric diploes with the Mg''_{Ti} at the centers of the octahedra. The reorientation of the $Mg''_{Ti} - V^{\bullet\bullet}_{O}$ defect pairs with inputted weak ac signals during the dielectric measurements can generate an inner attrition and increase energy dissipation. Thus, this reorientation behavior is contributive to increasing the dielectric loss. The dielectric loss fluctuation at relatively low MgO contents ($x \leq 20$) can be visualized as a result of the competition of these contributing factors. The steady dielectric loss decline when $x \geq 30$ indicates a prevailing role of the mixing effect on the parameter at relatively high MgO contents.

The tunability presented an identical variation trend with MgO content to that of the field coefficient, as shown in the inset of Fig. 7. This identity reveals a consistency of the two parameters in physical meaning, i.e., characterizing the efficiency of applied bias electric field in reducing dielectric constant. Compared with the pure $Ba_{0.6}Sr_{0.4}TiO_3$ specimen ($x = 0$), the composite specimens showed apparently reduced tunability values. The doping and mixing effects of added MgO are believed to account for this phenomenon. As is conceivable, the T_m shift of the $Ba_{0.6}Sr_{0.4}TiO_3$ phase in the composites to $-10\,^{\circ}C$ due to the Mg^{2+} doping served to decrease the tunability at room temperature. Moreover, the dispersion of nonferroelectric MgO phase with a low dielectric constant in the matrix of the composite specimens caused a field re-distribution effect and reduced the field exerted on the $Ba_{0.6}Sr_{0.4}TiO_3$ phase, which led to a lowering of the tunability. By comparison, the composite specimens showed a slight decline in the tunability with MgO content between $x = 10$–60. The specimen with $x = 60$ remained a roughly good tunability of 17.3%. Then one can argue that the tunability of the composite specimens is somewhat insensitive to the MgO content within the investigated composition range. This insensitivity is presumably due to the generally good connectivity between the $Ba_{0.6}Sr_{0.4}TiO_3$ grains in the composite specimens (Fig. 3).

As the definition implies, the variation of the FOM with MgO content depends on a compromise between the tunability and dielectric loss data. The composite specimen with $x = 60$ attained a FOM values of 127, which is higher than a previous result (80) measured under the identical conditions for 40 wt.% $Ba_{0.6}Sr_{0.4}TiO_3$/60 wt.% MgO composite ceramic prepared by microwave sintering [19]. The FOM value is also competitive to those (62–145) measured under the same conditions for 30 wt.% $Ba_{1-x}Sr_xTiO_3$/70 wt.% Mg_2TiO_4 ($x = 0.40$–0.55) composite ceramics prepared by the conventional method [33]. The FOM can be viewed as a criterion to assess the overall properties of nonlinear dielectrics [29]. The relatively high FOM value demonstrates superior nonlinear dielectric properties of the composite specimen prepared from the superfine $Ba_{0.6}Sr_{0.4}TiO_3$ and MgO powders.

4. Conclusions

Composites ceramics with a nominal composition of $Ba_{0.6}Sr_{0.4}TiO_3 + x$ wt.% MgO ($x = 0$–60) have been prepared using $Ba_{0.6}Sr_{0.4}TiO_3$ powder derived from the citrate method and superfine MgO powder. Adopting the superfine powders has been proved to be a feasible approach to improve the sinterability of the composites. The composites ceramics sintered at $1230\,^{\circ}C$ attained reasonable densification levels. The relatively low sintering temperature of the composites depressed the diffusion of Mg^{2+} into the lattice of the $Ba_{0.6}Sr_{0.4}TiO_3$ phase and, as a consequence, led to a small shift of the temperature for dielectric constant maximum (T_m) to $-10\,^{\circ}C$. The variation of nonlinear dielectric properties of the specimens with MgO content can be interpreted with respect to the doping and mixing effects caused by the MgO addition together with the connectivity between the $Ba_{0.6}Sr_{0.4}TiO_3$ grains in the composites. The mixing effect on the dielectric constant and the loss has been found to be predominant at relatively high MgO contents. The connectivity between the $Ba_{0.6}Sr_{0.4}TiO_3$ grains in the composite specimens is believed to be crucial to yielding good dielectric constant nonlinearity. These results may serve to be a clue to designing novel BST-based composite systems and controlling the preparation process. At room temperature, the composite specimen with $x = 60$ presented superior nonlinear dielectric properties, showing a reduced dielectric constant of 420 and a low dielectric loss of 0.14% at 10 kHz while maintaining a roughly good tunability of 17.3% and a high figure of merit of 127 at 10 kHz and 20 kV/cm.

Acknowledgements

This work was supported by the Ministry of Education (No. 108092), National Natural Science Foundation of China (A3 Foresight Program-50821140308) and Wuhan Science and Technology Bureau (No. 200851430485).

References

[1] L.C. Sengupta, S. Sengupta, Mater. Res. Innov. 2 (1999) 278.
[2] A.K. Tagantsev, V.O. Sherman, K.F. Astafiev, J. Venkatesh, N. Setter, J. Electroceram. 11 (2003) 5.
[3] B. Su, T.W. Button, J. Eur. Ceram. Soc. 21 (2001) 2777.
[4] B. Su, J.E. Holmes, C. Meggs, T.W. Button, J. Eur. Ceram. Soc. 23 (2003) 2699.
[5] D. Zhang, W.F. Hu, C. Meggs, B. Su, T. Price, D. Iddles, M.J. Lancaster, T.W. Button, J. Eur. Ceram. Soc. 27 (2007) 1047.
[6] R. Wu, P.Y. Du, W.J. Weng, G.R. Han, Mater. Chem. Phys. 97 (2006) 151.
[7] T. Tick, J. Perantie, H. Jantunen, A. Uusimaki, J. Eur. Ceram. Soc. 28 (2008) 837.
[8] R.K. Roeder, E.B. Slamovich, J. Am. Ceram. Soc. 82 (1999) 1665.
[9] B.L. Gersten, M.M. Lencka, R.E. Riman, J. Am. Ceram. Soc. 87 (2004) 2025.
[10] P.K. Sharma, V.V. Varadan, V.K. Varadan, Chem. Mater. 12 (2000) 2590.
[11] Y.B. Khollam, S.V. Bhoraskar, S.B. Deshpande, H.S. Potdar, N.R. Pavaskar, S.R. Sainkar, S.K. Date, Mater. Lett. 57 (2003) 1871.
[12] C. Shen, Q.F. Liu, Q. Liu, Mater. Lett. 58 (2004) 2302.
[13] Q. Xu, X.F. Zhang, Y.H. Huang, W. Chen, H.X. Liu, M. Chen, B.K. Kim, J. Alloys Compd. (2009) 125, doi:10.1016/j.jallcom.2009.05.
[14] Y. Chen, X.L. Dong, R.H. Liang, J.T. Li, Y.L. Wang, J. Appl. Phys. 98 (2005) 064107.
[15] X.J. Chou, J.W. Zhai, X. Yao, Appl. Phys. Lett. 91 (2007) 122908.
[16] J.J. Zhang, J.W. Zhai, X.J. Chou, X. Yao, J. Am. Ceram. Soc. 91 (2008) 3258.
[17] S.M. Ke, H.Q. Fan, W. Wang, G.C. Jiao, H.T. Huang, H.L.W. Chan, Compos. Part A-Appl. S 39 (2008) 597.
[18] W. Chang, L. Sengupta, J. Appl. Phys. 92 (2002) 3941.
[19] S. Agrawal, R. Guo, D. Agrawal, A.S. Bhalla, Ferroelectrics 306 (2004) 155.
[20] B. Su, T.W. Button, J. Appl. Phys. 95 (2004) 1382.
[21] T. Hu, H. Jantunen, A. Deleniv, S. Leppavuori, S. Gevorgian, J. Am. Ceram. Soc. 87 (2004) 578.
[22] U.C. Chung, C. Elissalde, M. Maglione, C. Estournes, M. Pate, J.P. Ganne, Appl. Phys. Lett. 92 (2008) 042902.
[23] R.H. Liang, X.L. Dong, Y. Chen, F. Cao, Y.L. Wang, Mater. Res. Bull. 41 (2006) 1295.
[24] R.H. Liang, X.L. Dong, Y. Chen, F. Cao, Y.L. Wang, Mater. Chem. Phys. 95 (2006) 222.
[25] X.H. Wang, W.Z. Lu, J. Liu, Y.L. Zhou, D.X. Zhou, J. Eur. Ceram. Soc. 26 (2006) 1981.
[26] B. Su, J.E. Holmes, B.L. Chen, T.W. Button, J. Electroceram. 9 (2002) 111.
[27] X.J. Chou, J.W. Zhai, X. Yao, J. Am. Ceram. Soc. 90 (2007) 2799.
[28] R.D. Shannon, Acta Crystallogr. A 32 (1976) 751.
[29] A. Feteira, D.C. Sinclair, I.M. Reaney, Y. Somiya, M.T. Lanagan, J. Am. Ceram. Soc. 87 (2004) 1082.
[30] K.M. Johnson, J. Appl. Phys. 33 (1962) 2826.
[31] C. Ang, Z. Yu, Phys. Rev. B 69 (2004) 174109.
[32] J.W. Liou, B.S. Chiou, Jpn. J. Appl. Phys. 36 (1997) 4359.
[33] P. Liu, J.J. Ma, L. Meng, J. Li, L.F. Ding, J.L. Wang, H.W. Zhang, Mater. Chem. Phys. 114 (2009) 624.